Computing Teichmüller Shape Space

Miao Jin[1], Wei Zeng[2], Feng Luo[3], and Xianfeng Gu[2]
[1]University of Louisiana at Lafayette [2]Stony Brook University [3]Rutgers University

***Abstract*— Shape indexing, classification, and retrieval are fundamental problems in computer graphics. This work introduces a novel method for surface indexing and classification based on Teichmüller theory. Two surfaces are conformal equivalent, if there exists a bijective angle-preserving map between them. The Teichmüller space for surfaces with the same topology is a finite dimensional manifold, where each point represents a conformal equivalence class, and the conformal map is homotopic to Identity. A curve in the Teichmüller space represents a deformation process from one class to the other.**

In this work, we apply Teichmüller space coordinates as shape descriptors, which are succinct, discriminating and intrinsic, invariant under the rigid motions and scalings, insensitive to resolutions. Furthermore, the method has solid theoretic foundation, and the computation of Teichmüller coordinates is practical, stable and efficient.

The algorithms for the Teichmüller coordinates of surfaces with positive or zero Euler numbers have been studied before. This work focuses on the surfaces with negative Euler numbers, which have a unique conformal Riemannian metric with -1 Gaussian curvature. The coordinates which we will compute are the lengths of a special set of geodesics under this special metric. The metric can be obtained by the curvature flow algorithm, the geodesics can be calculated using algebraic topological method.

We tested our method extensively for indexing and comparison of about one hundred of surfaces with various topologies, geometries and resolutions. The experimental results show the efficacy and efficiency of the length coordinate of the Teichmüller space.

***Index Terms*— Surface Classification, Surface Comparison, Shape Retrieval, Teichmüller Space, Hyperbolic Structure, Fuchsian Group, Ricci Flow, Riemann Uniformization**

I. Introduction

A. Motivation

Effective index and classification for shapes are very demanding with the dramatically increasing of 3D geometric models in online repositories, while also challenging. For a geometric algorithm, all the information that can be utilized is only the *topology and geometry* of the shape. But for human beings, shape classification and comparison involves the expectations of the *functionalities* of the objects. For example, for a human observer, the slatted chairs can still be quite similar even if they have a different number of slats; but for a computer, the objects are quite different because they have different topologies. Low level algorithms based on the geometric information need to be developed first to lay down the foundation for high level methods, which are closer to the human intelligence. The algorithms in both levels have fundamental importance. This work focuses on the algorithms solely based on the geometric information.

Shape descriptors can be constructed using different levels of geometric information. For example, surfaces can be classified by their topological properties, such as the number of the handles and the boundaries. Shapes can be differentiated more precisely by differential geometric properties, such as principle curvatures and fundamental forms. Topological descriptors are global, succinct and intuitive, but less discriminating; whereas differential geometric descriptors are local, redundant, but much more discriminating. The huge storage requirements prevent differential geometric descriptors from practical applications. This work introduces a novel approach for shape indexing and classification, with descriptors based on conformal geometry. In practice, it is hard to find two different types of shapes with handles sharing the same conformal descriptors, so descriptors based on conformal geometry are discriminating enough. What's more, conformal shape descriptors are intrinsic, independent of rotation, translation and scaling, and are also invariant to tessellation and isometric deformation. They are stable for deformations with small area stretching, like the posture change of a human skin surface, which changes slightly. They are efficient, easy to compute and compare. Therefore, we believe conformal geometric approach for shape classification and comparison has the potential for real applications.

B. Conformal Equivalence

A *conformal map*, also called an *angle-preserving map*, preserves local angles between two surfaces. while given two arbitrary surfaces with same topology, there may not exist conformal map between them, which is demonstrated as the angle distorted texture transferring from kitten model to rocker-arm model in figure 1 base on a map between them. They both are genus one surfaces, while no conformal map between them. For surfaces with same topology, We say they are *conformally equivalent* or belong to the same conformal class if there exists a bijective conformal map between them. Therefore, surfaces can be easily differentiated by conformal equivalence. All conformal classes form a space called Teichmüller space, which can be modeled as a finite dimensional manifold. Each surface has a unique coordinate in the space, and the dimension of the coordinates is determined by the topology of the surface. Two surfaces share the same coordinates in Teichmüller space if and only if they belong to the same conformal class.

An intuitive example is given by two planar annuli: we can scale them such that both of their outer radii are 1, while the inner radii are r_1 and r_2 respectively. There is no conformal map between them as long as $r_1 \neq r_2$. Therefore, the dimension of the conformal descriptors for all planar annuli is one, and the value is the inner radius after normalization. Another example is given by humans faces with three boundaries in Figure 2 (a), (b), (c). Their conformal descriptors are the geodesic lengths of their boundaries under hyperbolic uniformization metric, after we conformally map each face to two congruent right-angled hyperbolic polygons in

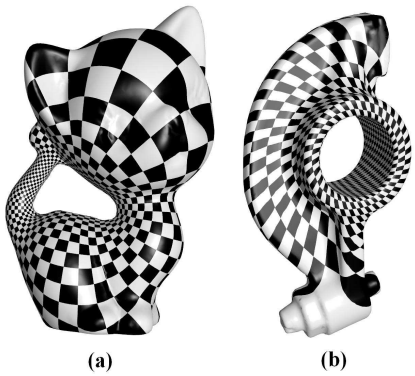

Fig. 1. A semi-conformal Map between genus one kitten model (a) and rocker-arm model (a) where the right corner angles on the kitten surface are distorted on the rocker-arm surface, which demonstrates that the map is not conformal.

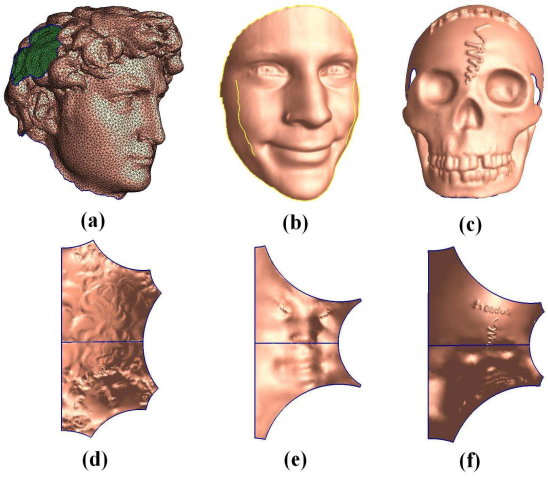

Fig. 2. Three human faces sharing the same topology (two holes annulus) are not conformally equivalent, which is verified by conformally mapping them to hyperbolic space and comparing their conformal descriptors: the edge lengths of the hyperbolic hexagon under hyperbolic uniformization metric.

Poincaré disk as shown in Figure 2 (d), (e), and (f). The dimension of their coordinates in Teichmüller space is three, the number of boundaries. Since those edge lengths are not equal, they do not belong to the same conformal class.

Conformal descriptors are invariant under conformal deformations, which include isometric deformations, rigid motions, and scaling. Figure 3 gives an example of a toy face (with different view points in Fig. 3 (a) and (b)) and its conformal descriptors (visualized as the three inner circles radii in Fig. 3 (c)). After isometric deformation of the toy face (with different view points in Fig. 3 (d) and (e)), the values of its conformal descriptors (visualized as the three inner circles radii in Fig. 3 (f)) do not change, which can be verified by the comparison of the three circles radii (between Fig. 3 (c) and (f)), and the difference error is under 0.0177.

This work proposes to classify surfaces based on Teichmüller space theory. In this work, we only consider oriented surfaces. We use (g,r) to represent the topological type of the surface, where g means the number of handles (genus), r the number of boundaries. After fixing the topology of the surfaces, all conformally equivalent classes form a finite dimensional manifold,

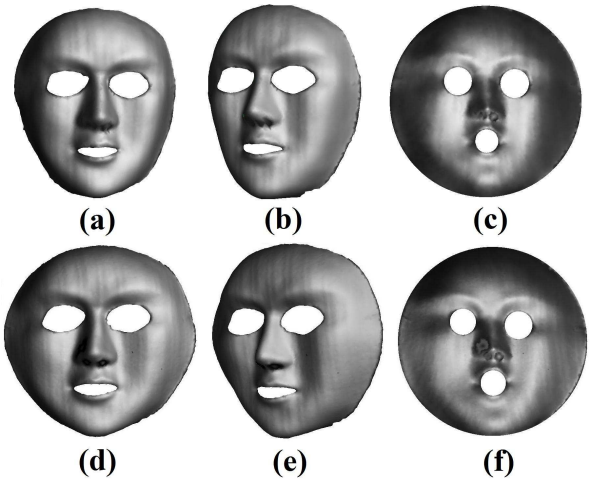

Fig. 3. Conformal descriptors are invariant under isometric deformations. The first row shows two views of the original surface and its conformal image; the second row shows two views of the deformed surface and its conformal image. Their conformal descriptors are visualized as the inner circles radii. Under isometric deformation, their conformal images are identical, which means their conformal descriptors are same.

the so-called *Teichmüller* space [1], where each point represents conformal equivalence class, and the conformal map is homotopic to Identity. A curve connecting different points represents a deformation process from one class to the other. The dimension of the Teichmüller space of negative Euler number surfaces with topological type $(g > 1, r)$ is $6g-5+3r$. Figure 4 illustrates the concept. The teapot surface has one handle and one boundary at the spout, therefore it is of topological type $(1,1)$, with 3 dimensions in Teichmüller space. The teapot in the middle is twisted with the deformation process indicated by the blue curve. The more the curve changes, the greater the distortion is. Another deformation process is depicted by the red curve where the teapot is scaled vertically. The two deformation paths are illustrated in both $\mathbb{R}^3$ and the Teichmüller space.

We briefly summarize the Teichmüller spaces for surfaces with different Euler numbers. The Euler number of type (g,r) is $2-2g-r$. The computational algorithms for the Teichmüller coordinates of surfaces with non-negative Euler numbers have been introduced before. This work focuses on surfaces with negative Euler numbers.

- The Teichmüller space for $(0,0)$ type surfaces, namely genus zero closed surfaces, has only one point. That means that all genus zero closed surfaces are conformally equivalent. In this case, we conformally map the surface to the unit sphere. By mapping different surfaces to the unit sphere, we can easily construct the conformal mapping between the two surfaces. The area distortion induced by the conformal mapping is called the *conformal factor*. In [2] we proved that the conformal factor and the mean curvature determine the surface uniquely up to a rigid rotation of the sphere. We use area distortion and mean curvature as shape descriptors for shape comparison purposes in [2].
- The Teichmüller space for $(0,1)$ type surfaces, namely genus zero surface with a single boundary, consists of a single point. All such surfaces can be mapped to the unit disk. Similarly, the conformal factor and mean curvature can be applied as shape descriptors.

- The Teichmüller space for $(1,0)$ type surfaces, namely tori, is two dimensional. The Teichmüller coordinates of a torus can be computed using global surface conformal parameterization method [3]. Basically, we can compute a holomorphic 1-form. By integrating the 1-form, we can map the universal covering space of the surface to the plane $\mathbb{R}^2$. Each fundamental domain is mapped to a parallelogram. The Teichmüller coordinates of the torus are the angle and the length ratio between two adjacent edges of the parallelogram. We refer readers to [3] for details.
- For all the other surfaces, the Euler numbers are negative. The coordinates in Teichmüller space can be computed in the following method. First, there exists a unique Riemannian metric, called the *hyperbolic uniformization metric*, which is conformal to the original metric of the surface and induces -1 constant Gaussian curvature everywhere. Furthermore, all the boundaries become geodesics under the uniformization metric. Two closed curves are *homotopic*, if one can deform to the other without leaving the surface. Under the hyperbolic uniformization metric, each homotopy class has a unique geodesic. We choose a special set of homotopy classes on the surface, then compute the unique geodesic in each class. The lengths of these geodesics are Luo's coordinates [4], which form the length coordinates of the surface in Teichmüller space. This work focuses on the computation of the length coordinates of surfaces with negative Euler numbers.

The major goal of this paper is to develop rigorous and practical algorithms to compute length coordinates of surfaces with negative Euler numbers in Teichmüller space. The major contributions of this work are:

1) it proposes a theoretical framework to model all negative Euler number surfaces in a shape space, Teichmüller space. The framework has deep roots in modern geometry and is practical for computation. It offers novel views and tools for tackling engineering problems.
2) it introduces a series of practical algorithms for computing length coordinates of negative Euler number surfaces in Teichmüller space. Those coordinates are with finite dimension, independent of scaling and rigid motion, and are also invariant to different tessellations. They can be applied for shape indexing to classify surfaces according to their conformal class.

The remainder of the paper is organized as follows. Section II contains a summary of related work, and the challenges in this area. Section III briefly introduces the theoretical background of Teichmüller space. Section IV describes our algorithms for computing the coordinates for general surfaces with negative Euler numbers in Teichmüller space. Section V presents results of our experiments on surface indexing and shape comparison, which evaluate the robustness, discriminability, and efficiency of our algorithms. We summarize the paper and point out future directions in the final section VI.

II. Related Work

Our work proposes to compute Teichmüller space coordinates as shape descriptors based on surface hyperbolic uniformization metric, which classify surfaces according to their conformal structures. Surfaces having the same descriptors share the same conformal structure, invariant to conformal deformations.

The research literature on shape descriptors is vast. A thorough review of shape descriptors is beyond the scope of current work. We will focus here only on recent shape descriptors which are most relevant to our work using conformal geometry, and methods for designing metrics by prescribed curvatures.

A. Shape Descriptors

For the application of 3D shape classification and matching, shape descriptors are to extract meaningful and simplified representations from the 3D model based on the geometric and topological characteristics of the object. As the name suggests, shape descriptors should be descriptive enough to be able to discriminate similar and dissimilar shapes. The interested reader is referred to [5], [6] and [7] for comprehensive surveys of different shape descriptors and evaluations of their performance.

Shape descriptors can be classified by the corresponding transformation groups, to which they are invariant. The following transformation groups are considered: *rigid motion, isometric transformation and conformal deformation*. The former groups are the subgroups of the latter ones. In the discussion, we focus on shape descriptors based on conformal geometry. There are many other shape descriptors invariant to the above transformation groups based on other methods. We only brief some of them.

1) Shape Descriptors Invariant to Conformal Deformations: Conformal structure is invariant to conformal deformations, which include isometric deformations and rigid motions. To the best of our knowledge, the first work proposed to use conformal structure for shape classification is [8], where the conformal structure is represented as period matrices. Later, geodesic spectrum of surfaces under their uniformization metrics are applied as the conformal structure descriptors in [9], which can be computed symbolically. A general framework for 3D surface matching is proposed in [10] and [11]. By conformally parameterizing the 3D surfaces to canonical 2D domains, the matching problem is greatly simplified. If the surfaces are conformally equivalent, then 2D mapping is an identity with appropriate boundary conditions.

2) Shape Descriptors Invariant to Isometric Transformations: Pose changes are a quasi-isometric transformation of the 3D mesh, in the sense that edge lengths do not change much as a result of the transformation. Pose-invariant Shape Descriptors are invariant under non-rigid isometric transformations, and tolerant quasi-isometric transformations. Pose-invariant shape descriptors based on conformal geometry is introduced in [12], where the histogram of the conformal factor computed from surface uniformization metric is applied as shape descriptor. This descriptor is intrinsic and pose-invariant.

Laplace-Beltrami operator is determined by the Riemannian metric. Therefore, most descriptors related to discrete laplace-Beltrami operators are also invariant to isometric deformations, and tolerant quasi-isometric deformations. For examples, Reuter et al. in [13] use the eigenvalues of Laplace-Beltrami operator; Rustamov in [14] uses the eigenvectors; Xiang et al. in [15] use the histogram of the solution to the volumetric Poisson equation which involves the Laplace-Beltrami operator.

3) Shape Descriptors Invariant to Rigid Motions: Shape descriptors invariant to rigid motions and based on conformal geometry are used in [2] and [16] for medical application purpose, where both conformal factor and mean curvature are considered.

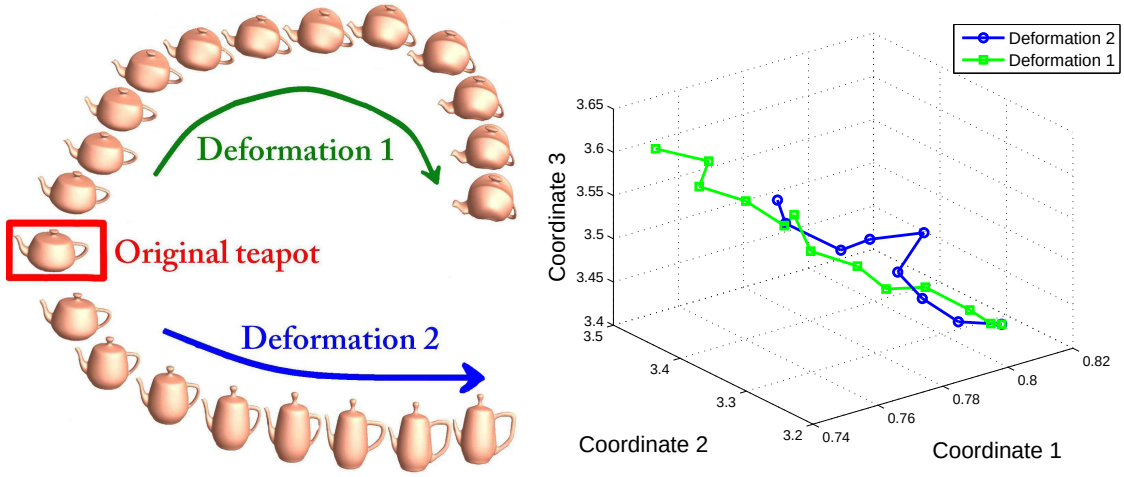

(a) Teapots deformed in Euclidean Space (b) Deformation paths in Teichmüller space

Fig. 4. The teapot surface with one handle and one boundary at the spout as shown in (a) has 3 dimensions in Teichmüller space, where each point represents one conformal equivalent class, and a curve connecting different points represents a deformation process from one class to the other as shown in (b).

Conformal factor itself fully determines the Riemannian metric of surfaces. After adding mean curvature, they two can determine the embedding of surfaces unique up to rigid motions with appropriate boundary conditions.

4) Other Shape Descriptors: There are many other shape descriptors invariant to isometric deformations based on Riemannian geometry. For example, those methods in [17]–[19] compute from surface geodesic distances. The method in [20] computes the diameter of the 3D shape at each point, and the average geodesic distance from each point to all other points. The histograms of the two functions are applied as the shape descriptors.

Many global or local features based, or graph based shape descriptors are invariant to rigid motions, while extra algorithms for feature and graph matching are necessary. We refer readers to [7] for more details.

B. Computing Metric from Prescribed Curvature

There are many algorithms for conformal surface parameterization in the literature. Comprehensive reviews can be found in [21] and [22]. Here we focus on approaches to compute conformal metrics from prescribed curvatures.

Richard Hamilton introduced Ricci flow for general Riemannian manifold in [23]. Later, Hamilton introduced surface Ricci flow in [24]. Perelman applied Ricci flow for the proof of Poincaré conjecture and Thurston's geometrization conjecture in [25]–[27]. A thorough introduction to Ricci flow can be found in [28] and [29].

A circle packing algorithm was introduced by Thurston in [30]. Bowers et al. and Stephenson et.al. improved the algorithm and built the software system, which are explained in [31], [32]. Chow and Luo discovered the intrinsic relation between Ricci flow and circle packing and laid down the theoretic foundation for discrete Ricci flow in [33], where the existence and convergence of the discrete Ricci flow were established. The variational approach to find constant curvature metrics on triangulated surfaces was pioneered in the works [34], [35], [36]. More recently, it appears in [37], [38] and [39]. Combinatorial Yamabe flow is introduced in [40].

The algorithm of discrete surface Ricci flow was given in [41], where the Ricci flows on meshes with spherical, Euclidean and hyperbolic background geometries are explained in details. Furthermore, Newton's method is directly applied to optimize the discrete Ricci energy. Optimal surface parameterization is formulated as a variational problem with respect to the target boundary curvatures in [42], and solved by constrained optimization algorithm.

Circle pattern method was proposed by Bobenko-Springborn in [43], [44], which used the notion of angle structures first introduced by Colin de Verdiére [45]. Based on [43], circle pattern algorithm was introduced in [46].

Metric scaling method is introduced in [47], which solved the discretized Poisson equation with the cot-Laplace operator induced by the original metric, then use harmonic maps to compute the embedding from the result metric. The method is linear and efficient.

Similar to the formulation of combinatorial Yamabe flow introduced in [39], [48] computes conformal equivalent metrics according to prescribed curvatures. The Yamabe energy in [39] is represented as an integration of a differential form, and formulated to an explicit form using Milnor's Lobachevsky function in [48]. The explicit formula of the Hessian matrix in [39] and [48] are equivalent, which is the cot-Laplace operator.

III. Teichmüller Space Theory

In this section, we briefly introduce the theoretical background of Teichmüller space theory, and the most directly related background knowledge in topology and hyperbolic geometry. For details, we refer readers to [49] for information on Algebraic topology, [50] for hyperbolic geometry, and [1] for Teichmüller space theory.

A. Topological Background

Let Σ be a surface, the closed curves in the surface are *homotopic* to each other if they can be deformed to each other without leaving the surface. Closed curves are classified by this

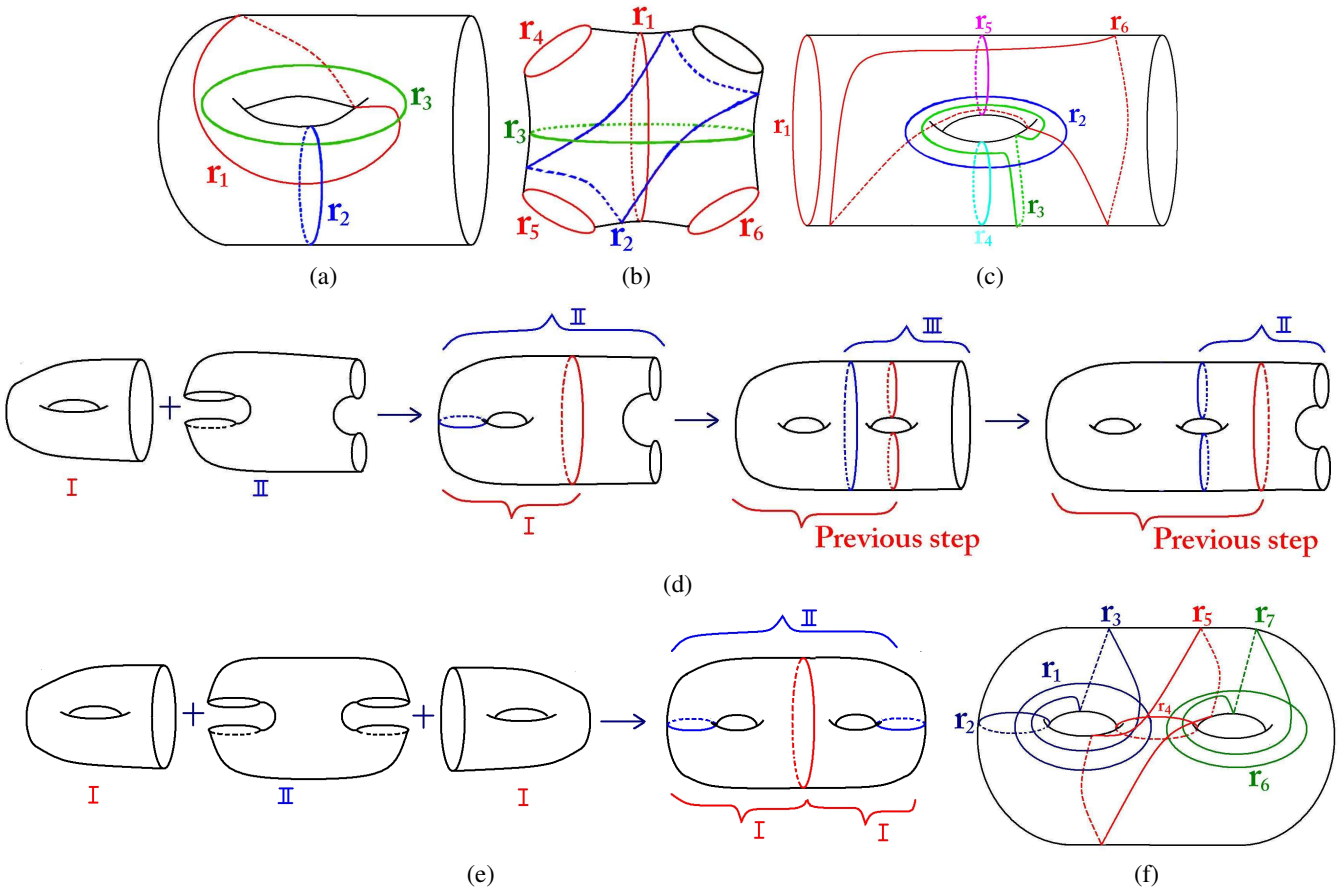

Fig. 5. (a) Building block I (b) Building block II (c) Building block III. For all of the three basic building blocks, the lengths of geodesics homotopic to the labeled curves determine the building block's metric. (d) Using building blocks I, II and III to build all surfaces: from left to right, using building block I and II to build genus one surface with two boundaries. Then adding building block III to build genus two surface with one boundary. Then adding building block II to build genus two surface with two boundaries. Repeating to get all surfaces. Note that marked curves on surface indicate the boundaries of overlapping part where two building blocks are glued together, and red and blue colors are used to distinguish boundaries coming from different building blocks. (e) The construction of genus two surface. (f) The geodesic lengths of the set of color labeled curves determine the metric of a genus two surface. Blue curves and green curves come from the first and the second Building blocks with type I; red curves come from building block with type II. Note that two of the curves for building block with type II and one for the second building block with type I are redundant and have been canceled off.

homotopic relation. The homotopy classes with the same base point form a group, which is called the *fundamental group*. Suppose Σ is of genus g, then there exists a set of canonical fundamental group generators $\{a_1,b_1,a_2,b_2,\cdots,a_g,b_g\}$, such that on each handle, there are two loops a_i,b_i. One loop a_i circles the hole and the other loop b_i loops around the tube. Figure 6(a) shows a set of canonical fundamental group generators of a genus two surface.

Suppose $\bar{\Sigma}$ is another surface, then $(\bar{\Sigma},\pi)$ is said to be a *covering space* of Σ if locally, π is a homeomorphism. If $\bar{\Sigma}$ is simply connected, then $(\bar{\Sigma},\pi)$ is the *universal covering space* of Σ.

For surface with negative Euler number, its universal covering space $\bar{\Sigma}$ is the hyperbolic space $\mathbb{H}^2$, which will be introduced in Section III-C. Its *Fuchsian transformations*, the transformations of the universal covering space to itself, $\phi:\bar{\Sigma}\to\bar{\Sigma}$, are hyperbolic rigid motions (Möbius transformations). Each Fuchsian transformation associates a homotopy class in the fundamental group in the following manner: giving a point p on Σ and $\bar{p}_0,\bar{p}_1\in\pi^{-1}(p)$ on the universal covering space $\bar{\Sigma}$. If ϕ is a Fuchsian transformation, such that $\phi(\bar{p}_0)=\bar{p}_1$, then any path $\bar{\gamma}\subset\bar{\Sigma}$ connecting $\bar{p}_0$ and $\bar{p}_1$ will be projected to a closed curve $\gamma=\pi(\bar{\gamma})$. Then we associate ϕ with the homotopy class of γ. Therefore, the Fuchsian transformation group is isotopic to the fundamental group of the surface.

B. Hyperbolic Uniformization Metric

A surface Σ in $\mathbb{R}^3$ has an induced Euclidean metric, denoted as $\mathbf{g}$. Suppose u is a function defined on Σ, $u:\Sigma\to\mathbb{R}$, then $e^{2u}\mathbf{g}$ is another metric conformal to the original one. If Σ has a negative Euler number, then it has a unique metric $\bar{\mathbf{g}}=e^{2\bar{u}}\mathbf{g}$, which is conformal to $\mathbf{g}$ and induces -1 Gaussian curvature at all interior points and 0 geodesic curvature at boundary points. The metric $\bar{\mathbf{g}}$ is called the *hyperbolic uniformization metric* of Σ.

In order to compute the hyperbolic uniformization metric, we need to find the function $\bar{u}:\Sigma\to\mathbb{R}$, which can be solved using *Ricci flow method*:

$$\frac{du(t)}{dt}=-2K(t),u(0)=0,$$

where $K(t)$ is induced by the metric of $e^{2u(t)}\mathbf{g}$. It has been proven that Ricci flow will converge $u(0)=0$ to $u(\infty)=\bar{u}$ which induces the hyperbolic uniformization metric [24], .

C. Hyperbolic Geometry

If Σ has a negative Euler number, then with uniformization metric, the universal covering space $\bar{\Sigma}$ can be isometrically embedded in the hyperbolic space $\mathbb{H}^2$.

There are two commonly used models for hyperbolic space, the *Poincaré disk* and the *upper half plane model*. The Poincaré disk is the unit disk in the complex plane, $|z| < 1$, with Riemannian metric $ds^2 = \frac{dzd\bar{z}}{(1-z\bar{z})^2}$. The rigid motions are the so-called *Möbius transformations* with the form $w = e^{i\theta}\frac{z-z_0}{1-\bar{z}_0 z}$. The hyperbolic lines are circular arcs perpendicular to the unit circle. The second model is the upper half plane model $y > 0$ with the metric $ds^2 = \frac{dzd\bar{z}}{y^2}$. The Möbius motions are of the form:

$$w = \frac{az+b}{cz+d}, a,b,c,d \in \mathbb{R}, ad-bc = 1.$$

A Möbius transformation in the upper half plane model is represented by its coefficients matrix. The coefficients matrix of the product of two Möbius transformations is equal to the product of their coefficients matrices.

The conformal transformation that maps the upper half plane to the Poincaré disk is $T = \frac{i-z}{i+z}$. Any Möbius transformation on the Poincaré disk ϕ can be converted to a Möbius transformation on the upper half plane as

$$T^{-1} \circ \phi \circ T. \tag{1}$$

The deck transformations of $\bar{\Sigma}$ on the hyperbolic disk are Möbius transformations, which form the *Fuchsian group* of Σ. Corresponding to the canonical fundamental group generators $\{a_1, b_1, a_2, b_2, \cdots, a_g, b_g\}$, the canonical Fuchsian group generators are referred as $\{\alpha_1, \beta_1, \alpha_2, \beta_2, \cdots, \alpha_g, \beta_g\}$. Suppose a loop has homotopy class $a_i b_j$, then its corresponding Fuchsian transformation is $\alpha_i \circ \beta_j$.

Suppose γ is a closed curve on a surface Σ with the hyperbolic uniformization metric, then there is a unique geodesic $\tilde{\gamma}$ homotopic to γ. Also, there is a unique Fuchsian transformation ϕ associated with the homotopy class of γ. The length of $\tilde{\gamma}$, $l(\tilde{\gamma})$, satisfies the following equation:

$$|trace(\phi)| = 2\cosh(\frac{l(\tilde{\gamma})}{2}).$$

In our implementation, we use this relation to compute the lengths of geodesics which are homotopic to a set of special closed loops on surfaces.

D. Teichmüller Space Coordinates

There are several coordinates defined in Teichmüller space. Here we adopt Luo's coordinates in [4] to avoid complicated computation of the twisting angles of Fenchel-Nielsen coordinates in [1].

In the following discussion, we use $\Sigma_{g,r}$ to represent a surface Σ with topological type (g,r), where g represents the genus, r means the number of boundaries.

Given a surface $\Sigma_{g,r}$ with negative Euler number, we can decompose the surface into three types of building blocks, as shown in Fig. 5 (a), (b) and (c). The procedure to build Σ from the building blocks is illustrated by Fig. 5 (d). We use $I \bigcap II$ to denote the process of gluing the block I to the block II. The gluing does not mean combining two blocks along their corresponding boundary curves, but by merging their overlapping regions. For example, in the first gluing step in the figure, the overlapping region of I and II is a two-holed annulus. From left to right, we use basic building blocks I and II so that $I \bigcap II$ is homeomorphic to $\Sigma_{1,2}$, a genus one surface with two boundaries; smoothly joining building block III, so that $\Sigma_{1,2} \bigcap III$ is homeomorphic to $\Sigma_{2,1}$, a genus two surface with one boundary; then joining building block II, so that $\Sigma_{2,1} \bigcap II$ is homeomorphic to $\Sigma_{2,2}$, a genus two surface with two boundaries; repeating this procedure, we can generate all types of surfaces with negative Euler surfaces. By this construction, a simple method is provided to define Luo's coordinates in Techmüller space for general surfaces.

For each building block, its conformal structure is determined by the lengths of geodesics homotopic to those red loops under the hyperbolic uniformization metric.

Although on general surfaces, in each homotopy class, there may be multiple geodesics, which are the locally shortest curves on surfaces. For surfaces with hyperbolic uniformization metric, the geodesic is unique in each homotopy class, which can be proved by Gauss-Bonnet theorem. We refer readers to [51] for details.

When two building blocks are glued together to form a new surface, non-homotopic loops on the original blocks may become homotopic on the resulting surface. After canceling off the redundant loops, the lengths of geodesics homotopic to remaining loops determine the conformal structure of the resulting surface, which are the coordinates of this surface in Techmüller space. For example, for a closed genus two surface, constructed from two building blocks of type I and one building block of type II as shown in Fig. 5 (e), its Techmüller coordinates are the lengths of geodesics homotopic to those loops marked with different colors as shown in Fig. 5 (f). Loops with the same color indicate that they come from the same building block. In general, for a surface $\Sigma_{g>1,r}$ with a negative Euler number, their Teichmüller coordinates are determined by the lengths of $6g+3r-5$ closed geodesics.

IV. Algorithms to Compute Length Coordinates in Teichmüller space

This section explains the algorithms for computing the Teichmüller space coordinates for surfaces with negative Euler numbers in details, represented as the lengths of a special set of geodesics under hyperbolic uniformization metric. The lengths of those geodesics can be symbolically computed from Fuchsian transformations, which require the generators of Fuchsian group, and Fuchsian group generators are calculated using the system of loops: canonical fundamental group generators. All of these computations are based on hyperbolic geometry.

The whole algorithms pipeline is as follows:

1) Compute hyperbolic uniformization metric of the surface, discussed in Sec. IV-A;
2) Compute Fuchsian group generators, discussed in Sec. IV-B;
3) Compute the coordinates in Teichmüller space, discussed in Sec. IV-C.

Following this pipeline, we discuss each step in detail.

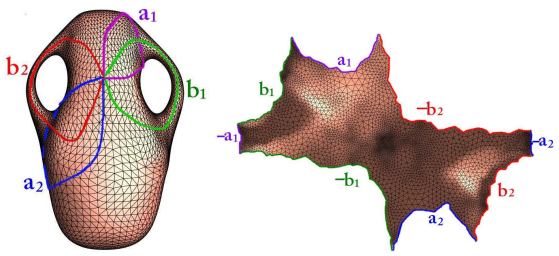

(a) (b)

Fig. 6. (a) Vase model with a set of canonical fundamental group generators marked with red. (b) Fundamental domain of vase model embedded in the Poincaré disk with the Hyperbolic Uniformization metric

A. Step 1. Compute Hyperbolic Uniformization Metric

In engineering fields, smooth surfaces are often approximated by discrete surfaces with triangulations. Since conformal deformation transforms infinitesimal circles to other infinitesimal circles and preserves the intersection angles among the circles, we can approximate discrete conformal deformation using circle packing metric introduced by Thurston in [30] by associating each vertex v_i with a cone of radius γ_i, each edge with edge weight Phi_{ij} which is the intersection angle of the two cones centered with the ending vertices v_i and v_j of that edge e_{ij}.

The discrete hyperbolic surface Ricci Flow on a discrete negative Euler number surface with circle packing metric is a process that the scaling of cone radius of Vertex v_i is proportionally evolving according to the discrete Gaussian curvature K_i of that vertex:

$$\frac{d\gamma_i}{dt} = -K_i \sinh \gamma_i, \tag{2}$$

while the intersection angles Φ_{ij} keeping unchanged. The final circle packing metric induces new metric of original surface approximated by edge lengths, which is conformal to original one but induces constantly negative Gaussian curvature, called hyperbolic uniformization metric. The discrete hyperbolic Ricci flow will converge exponentially. We refer the readers to [33] for theoretical proofs for the convergence of the discrete hyperbolic Ricci flow.

to compute discrete hyperbolic Ricci flow, we need to set the initial circle packing metric for a giving discrete surface, which approximates its original Euclidean metric as much as possible. Then we can use gradient descent method to solve Eqn. 2. The detailed algorithm can be found in Appendix Alg. 1.

We can further improve the convergence speed of comuting discrete hyperbolic Ricci flow with Newton's method. Letting $u_i = \ln \tanh \frac{\gamma_i}{2}$, we can define an energy form

$$f(\mathbf{u}) = \int_{\mathbf{u}_0}^{\mathbf{u}} \sum_{i=1}^{n} K_i du_i,$$

where $\mathbf{u} = (u_1, u_2, \cdots, u_n)$, $\mathbf{u}_0 = (0, 0, \cdots, 0)$ and $\frac{\partial f}{\partial u_i} = K_i$. Then the discrete hyperbolic surface Ricci Flow in Eqn. 2 is the negative gradient flow of this convex energy $f(\mathbf{u})$, and the solution of an energy optimization problem. So in practice we can use Newton's method to compute hyperbolic uniform metric with even faster convergence speed.

B. Step 2. Compute Fuchsian Group Generators in the Poincaré Disk Model

This step aims to compute the canonical Fuchsian group generators used for computing the geodesic lengths in the future step. There are several major steps to compute Fuchsian group generators:

1) Compute fundamental group generators, discussed in Sec. IV-B.1;
2) Isometric embed the mesh in the Poincaré disk, discussed in Sec. IV-B.2;
3) Compute the Fuchsian group generators, discussed in Sec. IV-B.3.

1) Compute Fundamental Group Generators: On a 'marked' surface, which means we have enumerated surface handles with h_1, h_2, h_3 etc., we pick a point on the surface as the base point (which can be any vertex on the surface), then for each handle h_i, we can uniquely decide a tunnel loop a_i which goes around the circle, a handle loop b_i which goes around the handle, and both of them go through the base point. By this way, We get a set of canonical fundamental group generators $\{a_1, b_1, a_2, b_2, \cdots, a_g, b_g\}$. Figure 6(a) shows a set of canonical fundamental group generators marked with different colors on vase model. The way to compute the canonical fundamental group generators has been studied in computational topology and computer graphics literature. We adopted the methods introduced in [52]. The surface S is then sliced open along the fundamental group generators to form a topological disk D, called fundamental domain. The boundary of D takes the form $\partial D = a_1 b_1 a_1^{-1} b_1^{-1} a_2 b_2 a_2^{-1} b_2^{-1} \cdots a_g b_g a_g^{-1} b_g^{-1}$.

2) Isometric Embedding in Hyperbolic Disk: Now we isometrically embed D onto the Poincaré disk using the uniformization metric computed from the first step. Let $\tau : D \to \mathbb{H}^2$ denote the isometric embedding.

First, we select an arbitrary face f_{012} from D as a starting face. Suppose the three edge lengths of the face are $\{l_{01}, l_{12}, l_{20}\}$, and the corner angles are $\{\theta_0^{12}, \theta_1^{20}, \theta_2^{01}\}$ under the uniform hyperbolic metric. We can simply embed the triangle as

$$\tau(v_0) = 0, \tau(v_1) = \frac{e^{l_{01}} - 1}{e^{l_{01}} + 1}, \tau(v_2) = \frac{e^{l_{02}} - 1}{e^{l_{02}} + 1} e^{i\theta_0^{12}}.$$

Second, we can embed all the faces which share an edge with the starting face. Suppose a face f_{ijk} is adjacent to the starting face, and vertices v_i, v_j have been embedded. A hyperbolic circle is denoted as $(\mathbf{c}, r)$, where $\mathbf{c}$ is the center, r is the radius. Then $\tau(v_k)$ should be one of the two intersection points of $(\tau(v_i), l_{ik})$ and $(\tau(v_j), l_{jk})$. Also, the orientation of $\tau(v_i), \tau(v_j), \tau(v_k)$ should be counter-clock-wise. In the Poincaré model, a hyperbolic circle $(\mathbf{c}, r)$ coincides with an Euclidean circle $(\mathbf{C}, R)$,

$$\mathbf{C} = \frac{2 - 2\mu^2}{1 - \mu^2 |\mathbf{c}|^2} \mathbf{c}, R^2 = |\mathbf{C}|^2 - \frac{|\mathbf{c}|^2 - \mu^2}{1 - \mu^2 |\mathbf{c}|^2},$$

where $\mu = \frac{e^r - 1}{e^r + 1}$. The intersection points between two hyperbolic circles can be found by intersecting the corresponding Euclidean circles. The orientation of triangles can also be determined using Euclidean geometry on the Poincaré disk.

Then, we can continue to embed faces which share edges with embedded faces in the same manner, until we embed the whole D onto the Poincaré disk.

Figure 6(b) shows the embedding of fundamental domain of vase model onto the Poincaré disk with its Hyperbolic Uniformization metric.

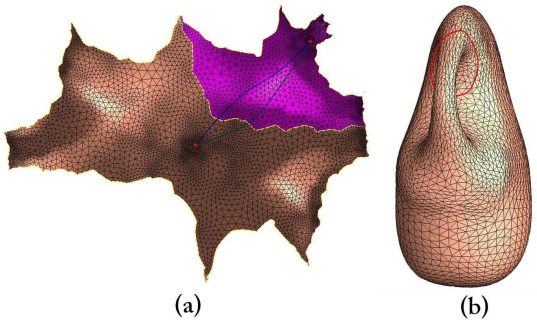

Fig. 7. (a) One Deck transformation maps the left period to the right one. (b) Two closed loops homotopic to the red one on the vase model lift as two blue Paths in the universal covering space.

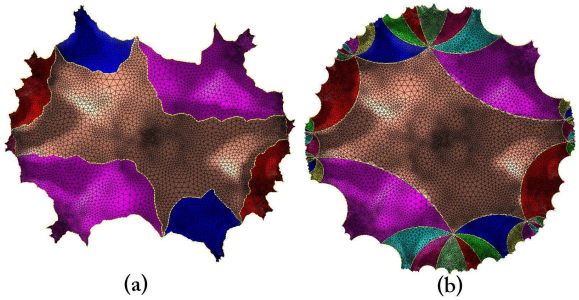

Fig. 8. (a) $2g$ Fuchsian group generators act on vase model, which are rigid motions in the hyperbolic space. Different color indicates different periods (fundamental domains). The generators maps the central period to the colored ones respectively. (b) A finite portion of the universal covering space of vase model, generated by the actions of Fuchsian group elements with boundaries marked with geodesics in hyperbolic space.

3) Fuchsian Group Generators: The embedding of a canonical fundamental domain for a closed genus g surface has $4g$ different sides, which induce $4g$ rigid transformations. These $4g$ rigid motions are the Fuchsian group generators.

Figures 6, 7, and 8 illustrate the process to compute Fuchsian group generators for a mesh with a negative Euler number. Let $\{a_1, b_1, \cdots, a_g, b_g\}$ be a set of canonical fundamental group generators as marked with red in Fig. 6(a), where g is the genus. The embedding of the vase's canonical fundamental domain in hyperbolic space has $4g$ sides, $\tau(a_1), \tau(b_1), \tau(a_1^{-1}), \tau(b_1^{-1}), ..., \tau(a_g), \tau(b_g), \tau(a_g^{-1}), \tau(b_g^{-1})$ (see Fig. 6(b) in Poincaré disk). There exists unique Möbius transformations α_k, β_k, which map the $\tau(a_k)$ and $\tau(b_k)$ to $\tau(a_k^{-1})$ and $\tau(b_k^{-1})$ respectively. Figure 7(a) shows one Fuchsian group generator acting on one copy of the fundamental domain of the vase model, which maps the $\tau(b_k)$ to $\tau(b_k^{-1})$. The two red points are the pre-images of a same point on the vase model. Paths connecting them are projected to closed loops homotopic to the red one on vase model, see Figure 7(b). And we will see the computation of the length of the geodesic homotopy to the loop in Fig. 7(b) only involves the Möbius transformation which maps $\tau(b_k)$ to $\tau(b_k^{-1})$. The Möbius transformations $\{\alpha_1, \beta_1, \alpha_2, \beta_2, \cdots, \alpha_g, \beta_g\}$ form a set of generators of Fuchsian group. Figure 8(a) shows eight copies of the fundamental domain of vase model tesselated coherently along boundaries by a set of Fuchsian group generators, and Fig. 8(b) shows more copies tesselated by Fuchsian transformations.

The following explains the details for computing β_1. Let the starting and ending vertices of the two sides be: $\partial\tau(b_1) = q_0 - p_0$ and $\partial\tau(b_1^{-1}) = p_1 - q_1$. Then the geodesic distance from p_0 to q_0 equals to the geodesic distance from p_1 to q_1 in the Poincaré disk. To align them, we first construct a Möbius transformation τ_0, which maps p_0 to the origin, and q_0 to a positive real number, with

$$\tau_0 = e^{-i\theta_0}\frac{z - p_0}{1 - \bar{p}_0 z}, \theta_0 = arg\frac{q_0 - p_0}{1 - \bar{p}_0 q_0}.$$

Similarly, we can construct another Möbius transformation τ_1, which maps p_1 to the origin, and q_1 to a real number, with $\tau_1(q_1)$ equals to $\tau_0(q_0)$. By composing the two, we get the final Möbius transformation $\beta_1 = \tau_1^{-1} \circ \tau_0$, which satisfies $p_1 = \beta_1(p_0)$ and $q_1 = \beta_1(q_0)$, and aligns the two sides together.

Then we convert the Fuchsian group generators from the Poincaré disk model to the upper half plane model using formula 1.

C. Compute Teichmüller Coordinates

Teichmüller coordinates are obtained by measuring the lengths of geodesics homotopic to a group of loops on surfaces under hyperbolic uniformization metric, and the geodesics are unique in each homotopy class since Gauss curvature is constantly negative everywhere. The major steps are as follows:

1) Decompose the surface to building blocks;
2) Determine the homotopy classes of the geodesics;
3) Compute the lengths of the geodesics in each homotopy class.

Surface with enumerated handles has fixed decomposition to building blocks with one handle by one handle as illustrated inversely in Figure 4(d) since the decomposition is purely based on topology. After redundant loops with the same homotopic class while belonging to different building blocks have been removed, our goal is to compute the lengths of geodesics homotopic to the remaining loops. For example, for a genus two surface, the remaining loops can be seen in Fig. 5 (f).

Since in the above steps, the canonical homology basis $\{a_1, b_1, a_2, b_2, \cdots, a_g, b_g\}$ and the corresponding Fuchsian group generator $\{\alpha_1, \beta_1, \alpha_2, \beta_2, \cdots, \alpha_g, \beta_g\}$ have been calculated already. To compute the length of geodesic homotopic to a loop γ on surface, we first use the algorithm in [49] to determine its homotopy class, which can be symbolically represented, for example: $\gamma = a_1 b_1 a_1^{-1} b_1^{-1}$. Then by mapping each a_i to α_i and b_j to β_j, we get its representation using corresponding Fuchsian transformations, still the previous example: $\phi_\gamma = \alpha_1\beta_1\alpha_1^{-1}\beta_1^{-1}$. Let the length of γ denoted as l_γ, and we use the matrix representation of ϕ_γ on the upper half plane. l_γ can be easily computed from the following relation: $|tr(\phi_\gamma)| = 2\cosh(\frac{l_\gamma}{2})$.

V. Implementation and Results

We have implemented the algorithms for computing the Teichmüller coordinates using C++ on the Windows platform. We verify our method by computing the shape coordinates on a large number of surface models with various topologies. The triangles count for the model ranging from thousands to tens of thousands. Due to the page limit, we only list part of our experimental results.

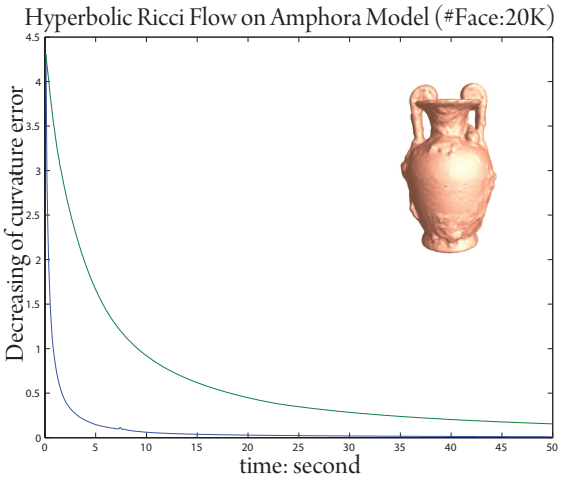

Fig. 9. Performance of curvature flow to compute hyperbolic uniformization metric for closed genus two amphora model with 20k faces. The horizontal axis represents time, and the vertical axis represents the maximal curvature error. The blue curves are for the Newton's method; the green curves are for the gradient descent method. The tests were carried out on a laptop with 1.7GHz CPU and 1G RAM. All the algorithms are written in C++ on a Windows platform without using any other numerical library.

A. Time Complexity

In the whole algorithm pipeline, the most time consuming is computing the hyperbolic uniformization metric. Figure 9 shows the statistics for the computation of hyperbolic uniformization metric for a closed genus two amphora model with 20k faces. The x-axis indicates the time, and the y-axis indicates the maximal curvature error. The green curve shows the steepest descendant method, and the blue curves show the Newton's method. For most models listed in the work, the time to compute their hyperbolic uniformization metrics is less than one minute.

B. Robustness

Teichmüller space coordinates are intrinsic properties of surfaces, independent of translation , rotation, scaling, and also insensitive to local noises, and the resolutions of the surface. We tested the robustness of our algorithm by computing for a model with different resolutions. Figure 10 illustrates one such an example. The vase model is tessellated using different resolutions, with the number of faces $5k$, $10k$, $20k$ and $40k$ respectively. We tested our Teichmüller coordinates algorithm on them. The results are listed in table I, including the mean average and standard deviation. As we can see, the relative error is less than 0.3%.

C. Surface Indexing and Classification

Teichmüller coordinates can be directly applied for indexing and classification of surfaces with the same topology. The distance among shapes in the Teichmüller space can be approximated directly using the Euclidean distances among their Teichmüller coordinates. In our experiments, we tested genus two closed surfaces and genus three closed surfaces.

For closed genus two surfaces, the dimension of Teichmüller space is seven. The Teichmüller coordinates for eight genus two teapot models are visualized in Fig. 11. The distances in the Teichmüller space among 23 genus two surfaces are listed in Table II. We cluster the shapes according to their Teichmüller distance. For example, Table III shows a neighborhood of the shape of the teapot7 model in the Teichmüller space. The surface closest to the teapot7 looks very similar to it. This matches our intuition.

	Coordinates of Vase Model						
Vase Model	1st	2nd	3rd	4th	5th	6th	7th
Face #: 5k	3.55027	0.99990	3.88055	5.55885	6.11438	3.33029	3.66071
Face #: 10k	3.55700	0.99832	3.88144	5.55611	6.11180	3.33369	3.66703
Face #: 20k	3.55805	0.99759	3.88316	5.55517	6.11112	3.33357	3.66713
Face #: 40k	3.55905	0.99559	3.88416	5.55417	6.11012	3.33367	3.66813
Average	3.55609	0.99785	3.88232	5.55607	6.11185	3.33280	3.66575
Std. Dev.	0.00343	0.00154	0.00141	0.00174	0.00157	0.00145	0.00294

TABLE I

COMPARISON OF COORDINATES OF VASE MODEL WITH DIFFERENT DENSITIES. THE DIMENSION OF TEICHMÜLLER SPACE COORDINATES FOR CLOSED GENUS TWO SURFACES IS SEVEN.

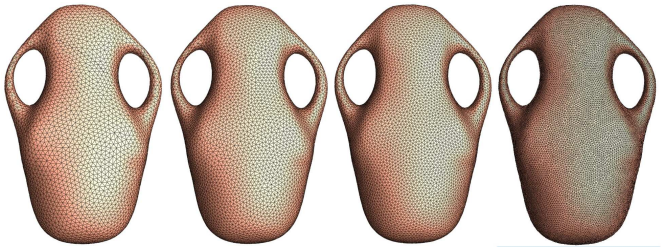

Fig. 10. Same model with different triangulation density: 5k, 10k, 20k and 40k. Comparison of Teichmüller space coordinates with different densities is listed in table I.

More examples are illustrated in Tables IV, V, VI, VII, VIII, and IX. For each table, we show models with the maximum and minimum distances to example model in Teichmüller space, based on table II. Furthermore, by examining Table II, we can also find that the knotty bottle model (the fifth model of the first row) is further away from all the others in the Teichmüller space, because its geometry is quite different from the others. Therefore, Teichmüller coordinates match our intuition.

For closed genus three surfaces, the dimension of their Teichmüller space is thirteen. We visualize the Teichmüller space coordinates for part of those models in Fig. 12. Table X lists the distances among those genus three surfaces in the Teichmüller space.

Models	Teapot5	Teapot6	Teapot2	Teapot4	Teapot1	Teapot0	Teapot3
distance							
	0.6468	1.1923	3.5202	4.1694	4.1742	4.5179	4.53

TABLE III

THE SORTED DISTANCES BETWEEN TEAPOT7 AND OTHER GENUS TWO MODELS IN TECHMÜLLER SPACE BASED ON TABLE II. HERE WE ONLY SHOW THE CLOSEST ONES.

distance																							
	4.09	5.39	3.22	4.49	6.69	2.22	2.16	2.21	2.39	2.32	4.38	3.87	4.88	3.51	3.52	3.42	3.25	4.02	3.29	3.20	3.44	3.26	3.41
		7.75	3.06	6.74	9.98	2.11	2.37	2.82	2.05	2.14	4.59	3.68	4.97	2.76	2.84	3.01	3.59	2.81	2.99	3.64	4.78	3.73	4.30
			4. 95	1.04	7.92	6.62	5.95	5.62	6.17	6.17	7.27	7.89	7. 34	7.46	6.56	6.48	5.61	6.97	6.32	5.63	4.72	5.56	5. 23
				3.94	8.99	2.47	1.73	1.64	1.85	1.83	4.27	4.27	4.56	3.08	3.43	3.22	2.37	3.84	3.02	2.52	2.75	2.43	2.64
					7.79	5.61	4.92	4.59	5.16	5.14	6.35	6.91	6.45	5.44	5.56	5.48	4.57	6.00	5.30	4.60	3.71	4.53	4.21
						8.48	8.48	8.35	8.61	8.62	9.27	9.13	9.57	8.75	8 .65	8.68	8.48	8.95	8.57	8.40	8.08	8.43	8.31
							0.83	1.51	0.73	0.71	4.05	3.15	4.51	2.09	1.92	1.51	2.27	2.42	1.51	2.36	3.59	2.43	3.12
								0.79	0.65	0.25	3.72	3.15	4.17	1.79	2.30	1.8 6	1.44	2.88	1.48	1.60	2.83	1.63	2.37
									1.40	0.92	3.10	2.83	3.52	2.51	3.02	2.64	1.54	3.62	2.14	1.26	2.13	1.28	1.61
										0.59	4.28	3.60	4.53	2.36	2.76	2.40	2.95	2.28	2.51	2.18	3.38	2.21	2.96
											3.71	3.07	4.16	1.63	2.20	1.76	1.62	2. 76	1.30	1.74	3.01	1.79	2.52
												1.62	0.64	5.21	5.71	5.40	4.61	6.26	4.83	4.30	4.03	4.35	3.88
													1.19	4.43	4.86	4.58	4.24	5.33	4.10	3.97	4.30	4.06	3.94
														5.67	6.19	5.88	5.02	6.73	5.31	4.92	4.82	4.86	4.63
															0.37	0.62	1.14	1.14	0.96	1.30	2.55	1.36	1.61
																0.63	1.63	0.63	0.96	1.80	2.9 7	1.87	2.58
																	1.25	1.09	0.60	1.45	2.68	1.49	2.23
																		2.20	0.87	0.34	1.47	0.29	1.03
																			0.53	1.39	3.57	2.45	3. 18
																				0.90	2.22	1.04	1.75
																					1.28	0.18	0.80
																						1.24	0.57
																							0.76

TABLE II

DISTANCES BETWEEN GENUS TWO SURFACES IN TECHMÜLLER SPACE.

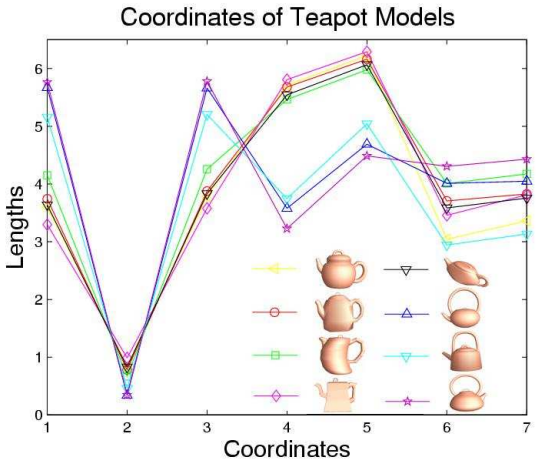

Fig. 11. **The dimension of Teichmüller space coordinates for closed genus two surfaces is seven. Here we visualize the Teichmüller space coordinates for teapots listed in table III.**

Distance							
0.60	0.62	0.63	1.09	5.48	5.88	6.48	8.68

TABLE IV

THE SORTED DISTANCES BETWEEN POT AND OTHER GENUS TWO MODELS IN TECHMÜLLER SPACE BASED ON TABLE II. HERE WE ONLY SHOW MODELS WITH MAXIMUM AND MINIMUM DISTANCES TO POT MODEL.

Distance							
0.53	0.60	0.87	0.90	5.30	5.31	6.32	8.57

TABLE V

THE SORTED DISTANCES BETWEEN VASE AND OTHER GENUS TWO MODELS IN TECHMÜLLER SPACE BASED ON TABLE II. HERE WE ONLY SHOW MODELS WITH MAXIMUM AND MINIMUM DISTANCES TO POT MODEL.

Distance							
1.04	4.72	4.95	5.23	7.46	7.75	7.89	7.92

TABLE VI

THE SORTED DISTANCES BETWEEN CUP AND OTHER GENUS TWO MODELS IN TECHMÜLLER SPACE BASED ON TABLE II. HERE WE ONLY SHOW MODELS WITH MAXIMUM AND MINIMUM DISTANCES TO POT MODEL.

Distance							
0.57	0.76	0.80	1.03	4.30	4.63	5.23	8.31

TABLE VII

THE SORTED DISTANCES BETWEEN WORLD CUP AND OTHER GENUS TWO MODELS IN TECHMÜLLER SPACE BASED ON TABLE II. HERE WE ONLY SHOW MODELS WITH MAXIMUM AND MINIMUM DISTANCES TO POT MODEL.

Distance							
0.59	0.65	0.73	1.40	4.53	5.16	6.17	8.61

TABLE VIII

THE SORTED DISTANCES BETWEEN TEAPOT3 AND OTHER GENUS TWO MODELS IN TECHMÜLLER SPACE BASED ON TABLE II. HERE WE ONLY SHOW MODELS WITH MAXIMUM AND MINIMUM DISTANCES TO POT MODEL.

Distance							
0.37	0.62	0.96	1.14	5.44	5.67	7.46	8.75

TABLE IX

THE SORTED DISTANCES BETWEEN EIGHT AND OTHER GENUS TWO MODELS IN TECHMÜLLER SPACE BASED ON TABLE II. HERE WE ONLY SHOW MODELS WITH MAXIMUM AND MINIMUM DISTANCES TO POT MODEL.

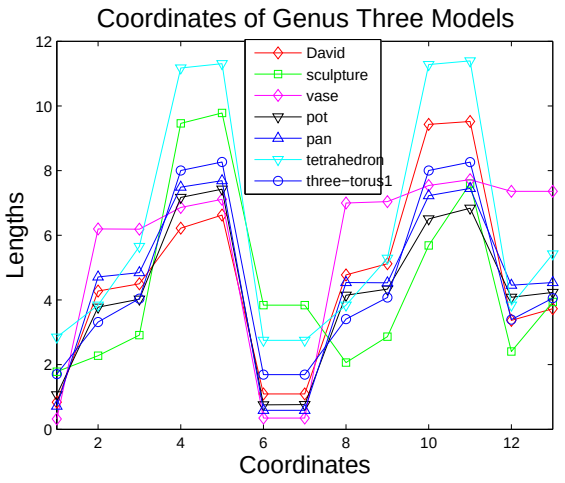

Fig. 12. **The dimension of Techmüller space coordinates for closed genus three surfaces is thirteen. Here we visualize the length coordinates of Techmüller space for part of genus 3 surfaces listed in table X.**

Models	three-torus	tetra-hedron	vase	David	sculp-ture	puppet	pot	pan	clip
Distance									
	6.43	5.56	13.19	8.16	7.60	8.21	9.19	9.16	5.95
		7 .07	8.36	3.89	5.11	2.16	3.02	3.27	8.50
			10.80	8.28	8.82	8.76	9.53	8.73	4.84
				7.29	12.17	7.50	7.03	5.83	12.02
					8.61	3.35	4.45	3.87	9.81
						6.52	6.66	7.49	10.56
							1.47	1.97	9.85
								1.79	10.50
									9.97

TABLE X
DISTANCES BETWEEN GENUS THREE SURFACES IN TECHMÜLLER SPACE.

VI. CONCLUSION AND FUTURE WORK

In this work, we propose a novel approach for surface indexing and classification based on Teichmüller space theory. Teichmüller space is a finite dimensional manifold, where each point represents a conformally equivalent class of surfaces, and a curve represents a deformation process from one shape to another.

As shape descriptors, Teichmüller coordinates are succinct, discriminating and intrinsic; invariant under the rigid motions and scalings, insensitive to resolutions. Furthermore, the method has solid theoretic foundation, and the computation of Teichmüller coordinates are practical, stable and efficient.

This work introduces a series of algorithms for computing the Teichmüller coordinates of surfaces with negative Euler numbers. The computational algorithms are theoretically sound and practically simple. The coordinates are algebraically deduced from lengths of geodesics homotopic to a set of special curves under the hyperbolic uniformization metric, which is obtained by using curvature flow method.

We verified our method on a large number of surfaces with negative Euler number and with various geometries, topologies and resolutions. We apply for surface indexing and classification applications. The extensive experiments demonstrate the efficacy, efficiency and robustness of our method.

Current work focuses on the computation of Teichmüller coordinates and approximates the geodesic distance between two points in the space by Euclidean distance. In theory, Teichmüller space has well-defined Riemannian metrics, and the geodesics between two shapes can be accurately computed. In the future, we will devise practical algorithms to compute the geodesics in Teichmüller spaces, and use geodesic distance to measure the difference between two shapes, to apply for surface deformation and surface morphing.

REFERENCES

[1] P. Buser, *Geometry and spectra of compact Riemann surfaces*. Birkhauser, 1992.

[2] X. Gu and B. C. Vemuri, "Matching 3d shapes using 2d conformal representations," in *MICCAI (1)* (C. Barillot, D. R. Haynor, and P. Hellier, eds.), vol. 3216 of *Lecture Notes in Computer Science*, pp. 771–780, Springer, 2004.

[3] X. Gu and S.-T. Yau, "Global conformal parameterization," in *Symposium on Geometry Processing* (L. Kobbelt, P. Schröder, and H. Hoppe, eds.), vol. 43 of *ACM International Conference Proceeding Series*, pp. 127–137, Eurographics Association, 2003.

[4] F. Luo, "Geodesic length functions and teichmüller spaces," *J.DIFFERENTIAL GEOMETRY*, vol. 48, p. 275, 1998.

[5] P. Shilane, P. Min, M. Kazhdan, and T. Funkhouser, "The princeton shape benchmark," pp. 167–178, 2004.

[6] N. Iyer, S. Jayanti, K. Lou, Y. Kalyanaraman, and K. Ramani, "Three-dimensional shape searching: state-of-the-art review and future trends.," *Computer-Aided Design*, vol. 37, no. 5, pp. 509–530, 2005.

[7] J. W. Tangelder and R. C. Veltkamp, "A survey of content based 3d shape retrieval methods," in *Multimedia Tools and Applications, in press*, 2008.

[8] X. Gu and S.-T. Yau, "Surface classification using conformal structures," in *ICCV*, pp. 701–708, 2003.

[9] M. JIN, F. LUO, S. YAU, and X. GU, "Computing geodesic spectra of surfaces," in *Proc. ACM Symposium on Solid and Physical Modeling (2007)*, pp. 387–393.

[10] S. WANG, Y. WANG, M. JIN, X. GU, and D. SAMARAS, "3d surface matching and recognition using conformal geometry," in *Proc. IEEE Conference on Computer Vision and Pattern Recognition*, no. 2, pp. 2453–2460, 2006.

[11] X. Gu, S. Wang, J. Kim, Y. Zeng, Y. Wang, H. Qin, and D. Samaras, "Ricci flow for 3d shape analysis," in *ICCV '07: IEEE International Conference on Computer Vision (ICCV'07)*, pp. 1–8, 2007.

[12] M. Ben-Chen and C. Gotsman, "Characterizing shape using conformal factors," in *Proceedings of Eurographics Workshop on Shape Retrieval*, (Crete), April 2008.

[13] M. Reuter, F.-E. Wolter, and N. Petnecke, "Laplacespectra as fingerprints for shape matching," in *Solid and Physical Modeling*, p. 101C106, 2005.

[14] R.-M. Rustamov, "Laplace-beltrami eigenfunctions for deformation invariant shape representation," in *Proc. Symposium on Geometry Processing*, 2007.

[15] P. Xiang, C.-O. Hua, F.-X. Gang, and Z.-B. Chuan, "Pose insensitive 3d retrieval by poisson shape histogram," in *Lecture Notes in Computer Science*, vol. 4488, pp. 25–32, 2007.

[16] Y. Wang, M.-C. Chiang, and P. M. Thompson, "Mutual information-based 3d surface matching with applications to face recognition and brain mapping," in *ICCV '05: Proceedings of the Tenth IEEE International Conference on Computer Vision (ICCV'05) Volume 1*, pp. 527–534, 2005.

[17] V. Jain and H. Zhang, "A spectral approach to shape-based retrieval of articulated 3d models," *Computer Aided Design*, vol. 39, pp. 398–407, 2007.

[18] A. Elad and R. Kimmel, "On bending invariant signatures for surfaces," *IEEE Transactions on Pattern Analysis and Machine Intelligence*, vol. 25, no. 10, pp. 1285–1295, 2003.

[19] T. Tung and F. Schmitt, "The augmented multiresolution reeb graph approach for content-based retrieval of 3d shapes," *International Journal of Shape Modeling*, vol. 11, no. 1, pp. 91–120, 2005.

[20] R. Gal, A. Shamir, and D. Cohen-or, "Pose oblivious shape signature," *IEEE Transactions on Visualization and Computer Graphics*, vol. 13, no. 2, p. 261C271, 2007.

[21] M. S. Floater and K. Hormann, "Surface parameterization: a tutorial and survey," in *Advances in Multiresolution for Geometric Modelling*, pp. 157–186, Springer, 2005.

[22] A. Sheffer, E. Praun, and K. Rose, "Mesh parameterization methods and their applications," *Foundations and Trends® in Computer Graphics and Vision*, vol. 2, no. 2, 2006.

[23] R. S. Hamilton, "Three manifolds with positive Ricci curvature," *Journal of Differential Geometry.*, vol. 17, pp. 255–306, 1982.

[24] R. S. Hamilton, "The ricci flow on surfaces," *Mathematics and general relativity*, vol. 71, pp. 237–262, 1988.

[25] G. Perelman, "The entropy formula for the Ricci flow and its geometric applications," Tech. Rep. arXiv.org, November 11 2002.
[26] G. Perelman, "Ricci flow with surgery on three-manifolds," Tech. Rep. arXiv.org, March 10 2003.
[27] G. Perelman, "Finite extinction time for the solutions to the Ricci flow on certain three-manifolds," Tech. Rep. arXiv.org, July 17 2003.
[28] B. Chow, P. Lu, and L. Ni, *Hamilton's Ricci Flow*, vol. 77 of *Graduate Studies in Mathematics*. AMS, 2006.
[29] B. Chow, S.-C. Chu, D. Glickenstein, C. Guenther, J. Isenberg, F. Luo, T. Ivey, D. Knopf, P. Lu, and L. Ni, *The Ricci flow: techniques and applications. Part I. Mathematical Surveys and Monographs*, vol. 135. Providence, RI: American Mathematical Society, 2007.
[30] W. P. Thurston, *Geometry and Topology of Three-Manifolds*. Princeton lecture notes, 1976.
[31] P. L. Bowers and M. K. Hurdal, "Planar conformal mappings of piecewise flat surfaces," *In Vis. and Math. III. Springer*, pp. 3–34, 2003.
[32] K. Stephenson, *Introduction To Circle Packing*. Cambridge University Press, 2005.
[33] B. Chow and F. Luo, "Combinatorial ricci flows on surfaces," *Journal Differential Geometry*, vol. 63, no. 1, pp. 97–129, 2003.
[34] C. de Verdiere Yves, "Un principe variationnel pour les empilements de cercles," *Invent. Math.*, vol. 104, no. 3, pp. 655–669, 1991.
[35] Braegger and Walter, "Kreispackungen und triangulierungen," *Enseign. Math.*, vol. (2) 38, no. 3-4, pp. 201–217, 1992.
[36] I. Rivin, "Euclidean structures on simplicial surfaces and hyperbolic volume," *Ann. of Math.*, vol. 2, no. 3, pp. 553–580, 1994.
[37] A. I. Bobenko and B. A. Springborn, "Variational principles for circle patterns and koebe's theorem," *Trans. Amer. Math. Soc.*, vol. 256, no. 2, pp. 659–689, 2004.
[38] G. Leibon, "Characterizing the delaunay decompositions of compact hyperbolic surfaces," *Geom. Topol.*, vol. 6, pp. 361–391, 2002.
[39] F. Luo, "Combinatorial yamabe flow on surfaces," *Commun. Contemp. Math.*, vol. 6, no. 5, pp. 765–780, 2004.
[40] F. Luo, "On teichmuller space of surface with boundary," *preprint*, 2005.
[41] M. Jin, J. Kim, F. Luo, and X. Gu, "Discrete surface ricci flow," *IEEE Transaction on Visualization and Computer Graphics*, 2008.
[42] Y.-L. Yang, J. Kim, F. Luo, and X. Gu, "Optimal surface parameterization using inverse curvature map," *IEEE Transaction on Visualization and Computer Graphics*, 2008.
[43] A. I. Bobenko and B. A. Springborn, "Variational principles for circle patterns and koebe's theorem," *Transactions of the American Mathematical Society*, vol. 356, pp. 659–689, 2004.
[44] A. Bobenko and P. Schröoder, "Discrete willmore flow," in *Symposium on Geometry Processing*, pp. 101–110, 2005.
[45] Y. C. de Verdière, "Un principe variationnel pour les empilements de cercles. (french) [a variational principle for circle packings]," *Invent. Math.*, vol. 104, no. 3, pp. 655–669, 1991.
[46] L. Kharevych, B. Springborn, and P. Schröder, "Discrete conformal mappings via circle patterns," *ACM Trans. Graph.*, vol. 25, no. 2, pp. 412–438, 2006.
[47] M. Ben-Chen, C. Gotsman, and G. Bunin, "Conformal flattening by curvature prescription and metric scaling," *Computer Graphics Forum (Proc. Eurographics 2008)*, vol. 27, no. 2, p. to appear, 2008.
[48] B. Springborn, P. Schröder, and U. Pinkall, "Conformal equivalence of triangle meshes," *SIGGRAPH 2008*, 2008.
[49] J.R.Munkres, *Elements of Algebraic Topology*. Addison-Wesley Co., 1984.
[50] W. P. Thurston, *Three-Dimensional Geometry and Topology*. Princeton University Presss, 1997.
[51] T. S. Mika Seppala, *Geometry of Riemann surfaces and Teichmüller spaces*. North-Holland Math Stud, 1992.
[52] C. Carner, M. Jin, X. Gu, and H. Qin, "Topology-driven surface mappings with robust feature alignment," in *IEEE Visualization*, pp. 543–550, 2005.

APPENDIX

Algorithm 1 Compute Hyperbolic Uniformization Metric

for each vertex v_i **do**
  for each face f_{ijk} adjacent to vertex v_i **do**
    compute a radius for v_i:

$$\gamma_i^{jk} = \frac{l_{ki} + l_{ij} - l_{jk}}{2},$$

    $\{l_{ij}, l_{jk}, l_{ki}$: lengths of the edges e_{ij}, e_{jk}, e_{ki} on $f_{ijk}\}$
  end for
  average the radii from the faces adjacent to v_i:

$$\gamma_i = \frac{1}{m} \sum_{f_{ijk} \in F} \gamma_i^{jk},$$

  $\{m$: *the number of the adjacent faces to* $v_i\}$
end for
{*Associating each vertex with a cone of radius which approximates the original Euclidean metric.*}
for each edge e_{ij} **do**
  compute edge weight $\Phi_{ij}(e_{ij})$ from γ_i, γ_j using hyperbolic cosine law:

$$\cosh l_{ij} = \cosh\gamma_i \cosh\gamma_j + \sinh\gamma_i \sinh\gamma_j \cos\Phi_{ij}$$

end for
{*Assigning an edge weight to each edge based on the intersection angle of the two cones centered with the two ending vertices of the edge.*}
repeat
  for each edge e_{ij} **do**
    compute edge length l_{ij} from the current vertices radii γ_i and γ_j, and the fixed edge weight Φ_{ij} using the inverse of hyperbolic cosine law.
  end for
  {*Computing edge length from current circle packing metric.*}
  for each face f_{ijk} **do**
    for all face f_{ijk} **do**
      Compute the corner angles θ_i^{jk} from the current edge lengths using hyperbolic cosine law.
    end for
  end for
  for each vertex v_i **do**
    Compute the discrete Gaussian curvature K_i on v_i.
    if v_i is interior vertex **then**

$$K_i = 2\pi - \sum_{f_{ijk} \in F} \alpha_i^{jk}, \tag{3}$$

      $\{\alpha_i^{jk}$: corner angle attached to vertex v_i in the face $f_{ijk}\}$
    else if v_i is boundary vertex **then**

$$K_i = \pi - \sum_{f_{ijk} \in F} \alpha_i^{jk}, \tag{4}$$

    end if
  end for
  for each vertex v_i **do**
    Update γ_i of each vertex v_i,

$$\gamma_i = \gamma_i + \varepsilon(\bar{K}_i - K_i),$$

    $\{\bar{K}_i$: target Gaussian curvature$\}$
  end for
until $\max|\bar{K}_i - K_i| < \delta$
{*Optimizing discrete hyperbolic Ricci energy with steepest descent method.*}